THE ASTROPHYSICAL JOURNAL, 458:610–620, 1996 February 20

SPATIAL VARIATION OF THE 3.29 AND 3.40 MICRON EMISSION BANDS WITHIN REFLECTION NEBULAE AND THE PHOTOCHEMICAL EVOLUTION OF METHYLATED POLYCYCLIC AROMATIC HYDROCARBONS

C. JOBLIN,[1] A. G. G. M. TIELENS,[1] L. J. ALLAMANDOLA,[1] AND T. R. GEBALLE[2]
Received 1995 April 6; accepted 1995 July 28

ABSTRACT

Spectra of 3 μm emission features have been obtained at several positions within the reflection nebulae NGC 1333 SVS3 and NGC 2023. Strong variations of the relative intensities of the 3.29 μm feature and its most prominent satellite band at 3.40 μm are found. It is shown that (i) the 3.40 μm band is too intense with respect to the 3.29 μm band at certain positions to arise from hot band emission alone, (ii) the 3.40 μm band can be reasonably well matched by new laboratory spectra of gas-phase polycyclic aromatic hydrocarbons (PAHs) with alkyl ($-CH_3$) side groups, and (iii) the variations in the 3.40 μm to 3.29 μm band intensity ratios are consistent with the photochemical erosion of alkylated PAHs. We conclude that the 3.40 μm emission feature is attributable to $-CH_3$ side groups on PAH molecules. We predict a value of 0.5 for the peak intensity ratio of the 3.40 and 3.29 μm emission bands from free PAHs in the diffuse interstellar medium, which would correspond to a proportion of one methyl group for four peripheral hydrogens. We also compare the 3 μm spectrum of the proto–planetary nebula IRAS 05341+0852 with the spectrum of the planetary nebula IRAS 21282+5050. We suggest that a photochemical evolution of the initial aliphatic and aromatic hydrocarbon mixture formed in the outflow is responsible for the changes observed in the 3 μm emission spectra of these objects.

Subject headings: dust, extinction — infrared: ISM: lines and bands — molecular processes — reflection nebulae

1. INTRODUCTION

The 3.1–3.7 μm (3200–2700 cm^{-1}) spectral region of objects which emit the well-known features at 3.3, 6.2, 7.7, 8.6, and 11.3 μm can be thought of as consisting of three components: a band at 3.29 μm (3040 cm^{-1}) which is generally the most prominent feature in this region; a broad, weak plateau which extends from about 3.2 to 3.6 μm (3100–2780 cm^{-1}); and a series of weaker features superimposed on the plateau (Geballe et al. 1985; de Muizon et al. 1986; Geballe et al. 1989; Jourdain de Muizon, d'Hendecourt, & Geballe 1990a). In the PAH model, these features are thought to come from free, vibrationally excited, polycyclic aromatic hydrocarbons (PAHs) as they relax by fluorescence at their characteristic vibrational frequencies (for reviews, see Allamandola, Tielens, & Barker 1989; Puget & Léger 1989). The 3.29 μm (3040 cm^{-1}) band is assigned to the $v = 1 \rightarrow 0$ aromatic C-H stretching transition. The plateau and superimposed features have been attributed to several types of transitions including overtone and combination bands involving lower lying fundamental vibrations, and $\Delta v = -1$ C-H stretching transitions originating in v levels higher than 1 (hot band emission; Barker, Allamandola, & Tielens 1987, Allamandola et al. 1989). Another candidate for these features is the C-H stretch emission from aliphatic side groups attached to PAHs (Jourdain de Muizon, d'Hendecourt, & Geballe 1990b).

The observational program described in this paper was carried out to better characterize the spectroscopic details of the 3 μm emission. In order to test the variations of the three main components as a function of environment rather than object type, spectra were measured at various positions within two well-studied, extended sources: the reflection nebulae NGC 1333 and NGC 2023.

2. OBSERVATIONS AND DATA REDUCTION

Infrared spectra of selected positions within NGC 1333 (Fig. 1) and NGC 2023 (Fig. 2) were obtained at the United Kingdom 3.8 m Infrared Telescope (UKIRT) on Mauna Kea on 1989 December 16 and 17 and 1990 November 29 and 30 (UT). An observing log is provided in Table 1. All measurements of these objects utilized the seven-channel scanning grating spectrometer, CGS2, which provided an approximately constant resolution of $\sim$0.008 μm across the wavelength range. The entrance aperture of the spectrometer was a 5″ diameter circle. Spectra were obtained in a chop/nod mode and were sampled every $\frac{1}{3}$ resolution element, with nodding occurring after the entire spectral range was scanned. Chop throws and orientations were chosen to minimize contamination of the spectra by emission in reference sky positions. Pointing was achieved by offsetting from nearby stars and was accurate to better than 1″. Weather conditions were not ideal, with high winds and/or high humidity in 1989 and high humidity and thin cirrus in 1990.

The standard stars listed in Table 1 were observed on the same nights and at approximately the same air masses as the sources for which they were used. Data reduction involved dividing source spectra by a standard spectrum and multiplying the ratio by a blackbody function corresponding to the effective temperature and brightness of the standard star. This technique was effective in canceling telluric absorption lines, with the exception of the strong absorption of CH_4 near 3.315 μm and H_2O at 3.21 μm. Narrow spectral features near these wavelengths in Figures 3 and 4 should be disregarded. The final spectra have been smoothed by a Gaussian of FWHM 1.5 data points, lowering the resolution to about 0.009 μm. The flux calibrations are believed to be accurate to $\pm$20%.

[1] NASA Ames Research Center, MS: 245-6, Moffett Field, CA 94035.
[2] Joint Astronomy Centre, 660 N. A'ohoku Place, Hilo, HI 96720.

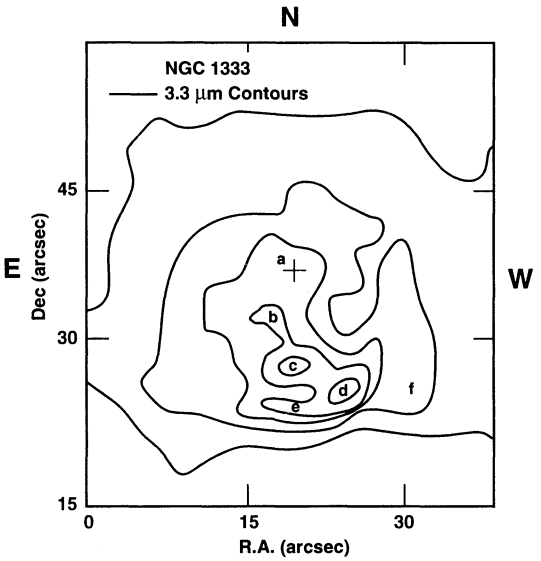

FIG. 1.—Contour map of the 3.29 μm emission feature measured by Burton et al. (1988) in the reflection nebula NGC 1333 SVS3. The letters *a–f* indicate the positions which have been observed within the nebula and whose spectra are shown in Fig. 3. The position *a* is centered on the star, SVS3, which is indicated by a cross.

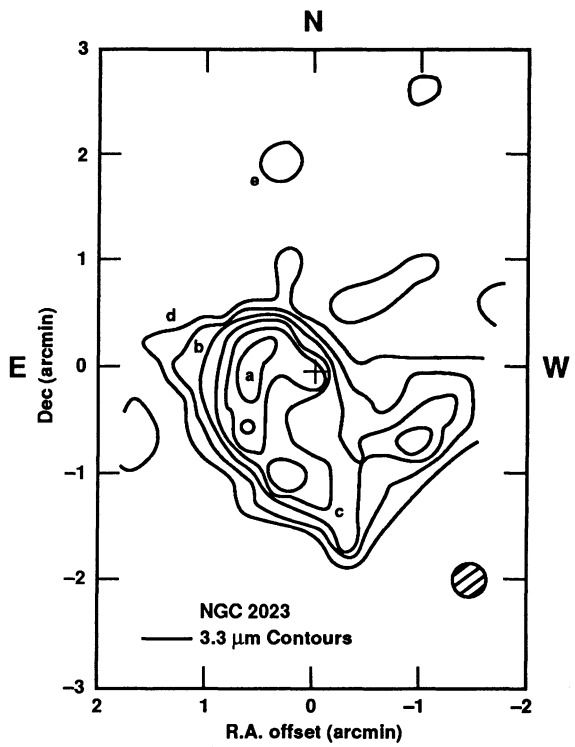

FIG. 2.—Contour map of the 3.29 μm emission feature measured by Gatley et al. (1987) in the reflection nebula NGC 2023. The contour interval is 7×10^{-20} W cm^{-2} per beam. The letters *a–e* indicate the different position which have been observed within the nebula and whose spectra are shown in Fig. 4. The cross indicates the position of the exciting star, HD 37903.

3. RESULTS

3.1. *Description of the Spectra*

The measured spectra are shown in Figures 3 and 4 in order of increasing angular distance from the illuminating star, in NGC 1333 and NGC 2023, respectively.

In NGC 1333, all spectra show the aromatic C-H stretching band at 3.292 ± 0.002 μm. The feature to continuum ratio varies between 11 and 37 off the star (Table 2). The values are comparable to those measured by Geballe et al. (1989) in the Orion Bar but are larger than the values (less than 15) measured in several reflection nebulae by Sellgren, Werner, & Dinerstein (1983). The width of the 3.29 μm feature is 0.043 ± 0.003 μm for all positions except (0, 0) and (−11, −11), where it could be less (0.036 ± 0.003 μm). The main satellite band peaks at 3.403 ± 0.003 μm in positions at which it is bright. Spectra at positions (2, 5), (0, −9), (−6, −11), and (0, −13) show shoulders on the long-wavelength side of the 3.40 μm band; the shoulder is especially prominent 9″ south of SVS3 (Fig. 3*c*). We note that a shoulder at 3.43 μm is also observed at position 4 in the Orion Bar (Geballe et al. 1989) and in the planetary nebula IRAS 21282+5050 (Jourdain de Muizon et al. 1990a). In the brighter positions, weak features may be observed at 3.463 μm at positions (0, −13) and (+2, −5), and at 3.515 ± 0.002 μm at positions (0, −13), (+2, −5), and (0, −9). These subfeatures have been detected in several other sources (de Muizon et al. 1986; Geballe et al. 1989; Jourdain de Muizon et al. 1990a). Another feature, observed at 3.232 ± 0.001 μm at positions (0, −13), (+2, −5), (−6, −11), and (−11, −11), is identified as the 1−0 O(5) line of H_2.

In NGC 2023, the 3.29 μm feature is strong at only two of the observed positions, (38, 0) and (−11, −78), and the spectrum between 3.35 and 3.65 μm was only recorded for these two positions. The main emission bands are observed at 3.292 ± 0.001 with a 0.038 ± 0.003 μm FWHM, and at 3.401 ± 0.001 μm with a 0.033 μm FWHM. Details of the profile of this band are not clear, owing to the low signal-to-noise ratio. There is evidence at position (−11, −78) for the H_2 line at 3.23 μm.

We have decomposed the observed spectra into three components: the 3.29 μm feature, the 3.40 μm feature, and an underlying plateau which extends from about 3.2 to 3.6 μm (Figs. 3–4). Peak intensities of the three components in NGC 1333 and NGC 2023 are listed in Table 2 and compared with other sources from the literature in which spatial measurements are available: the Orion Bar and the Red Rectangle (Geballe et al. 1989).

Table 2, as well as Figures 3–4, shows that the intensities of the three components vary with distance from the star. The most remarkable effect is observed for the ratio of the 3.40 μm and the 3.29 μm band intensities. This ratio decreases for positions closer to the illuminating star, a behavior first noted by Geballe et al. (1989) in the Orion Bar and the Red Rectangle. The spatial behavior of the plateau relative to that of the other features is more difficult to characterize. As discussed below, its enhanced intensity at the positions where the 3.40 μm band is strong may be caused by an additional spectrally broad contribution to it from this band. In view of the difficulty to characterize the plateau, we focus on the 3.29 and 3.40 μm bands in the remainder of this paper.

3.2. *Description of the Observed Regions*

In order to better understand the variations of the 3.29 and 3.40 μm band intensities, we give in the following a short description of the radiation field and density which are thought to prevail in the observed regions. The *G* values of the UV field intensity at each position are summarized in Table 2. They represent the integrated flux between 6 and 13.6 eV and are

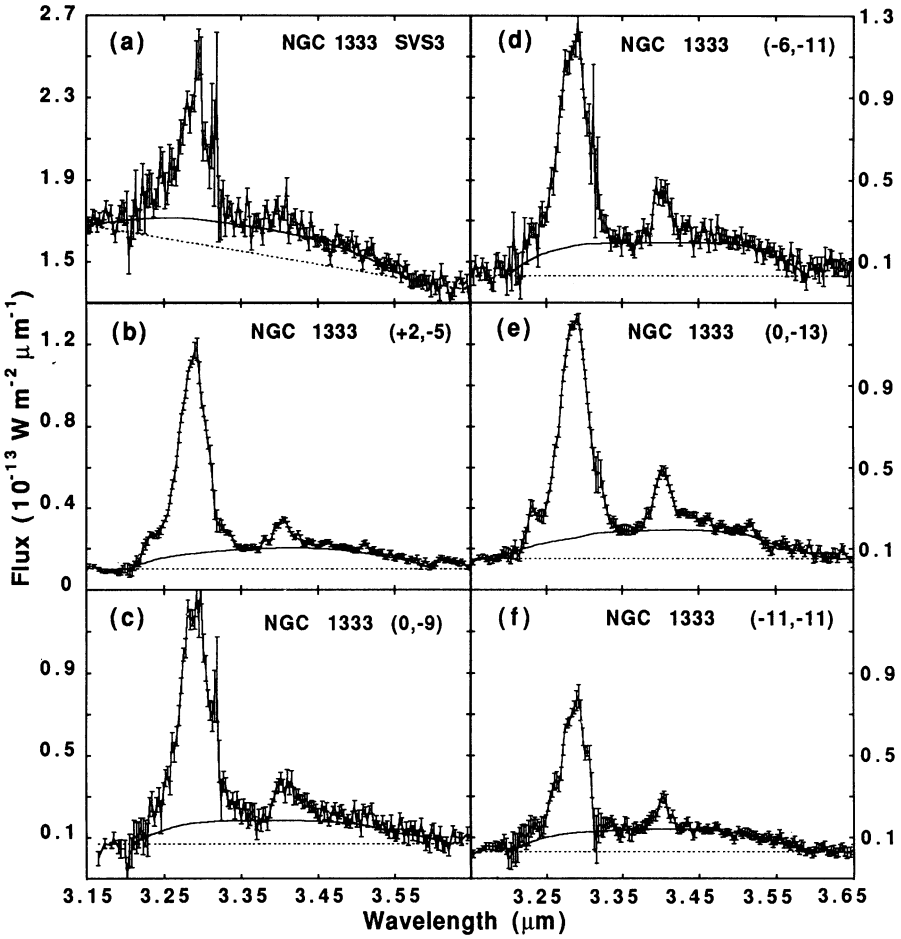

FIG. 3.—The 3.15–3.65 μm spectra measured at different positions within the reflection nebula NGC 1333 SVS3. The letters *a–f* correspond to the positions shown in Fig. 1 and are ordered by increasing distance from the star, SVS3. All spectra exhibit the 3.29 μm band, its satellite band at 3.40 μm, and the underlying 3.2–3.6 μm plateau which is arbitrarily defined by the solid line. The dotted line is taken as the continuum.

normalized to the average value for the interstellar medium, $G_o = 1.6 \times 10^{-3}$ ergs cm^{-2} s^{-1} (Habing 1968). The local value of the radiation field depends on the distance from the source (dilution factor) and on the local extinction. The first factor affects the total number of UV photons but preserves their spectral distribution, whereas the second factor also modifies the spectral distribution depending on the dust extinction properties.

3.2.1. *NGC 1333*

This reflection nebula is located 500 pc from Earth. The illuminating star SVS3 is of spectral type B6 with $T = 13{,}000$ K, and $L = 360\ L_\odot$ (Harvey, Wilking, & Joy 1984). The stellar

TABLE 1

OBSERVING LOG

Source Name	Offset (E, N)	UT Date	Spectral Coverage (μm)	Total Integration Time (minutes)	Chop Throw	Standard Star[a]
NGC 1333/SVS3	(0″, 0″)	1989 Dec 16	3.15–3.65	33	30″ E-W	BS 544
	(0, −9)	1989 Dec 16	3.15–3.65	53	30 E-W	BS 544
	(−6, −11)	1089 Dec 17	3.00–3.75	86	30 E-W	BS 544
	(+2, −5)	1990 Nov 29	3.15–3.65	33	60 E-W	BS 788
	(+2, −5)	1990 Nov 30	3.15–3.65	33	60 E-W	BS 788
	(−11, −11)	1990 Nov 29	3.15–3.65	33	60 E-W	BS 788
	(0, −13)	1990 Nov 30	3.15–3.65	33	60 E-W	BS 788
NGC 2023/HD 37903.....	(+38, 0)	1990 Nov 30	3.18–3.57	134	100 SE-NW	BS 1543
	(+80, +30)	1990 Nov 30	3.24–3.34	15	100 SE-NW	BS 1543
	(+62, +15)	1990 Nov 30	3.24–3.34	15	100 SE-NW	BS 1543
	(+33, +105)	1990 Nov 30	3.24–3.34	10	100 SE-NW	BS 1543
	(−11, +78)	1990 Nov 30	3.18–3.57	100	100 SE-NW	BS 1543

[a] BS 544: $L = 2.20$, $T = 6400$ K; BS 788: $L = 3.53$, $T = 6000$ K; BS 1543: $L = 2.05$, $T = 6500$ K.

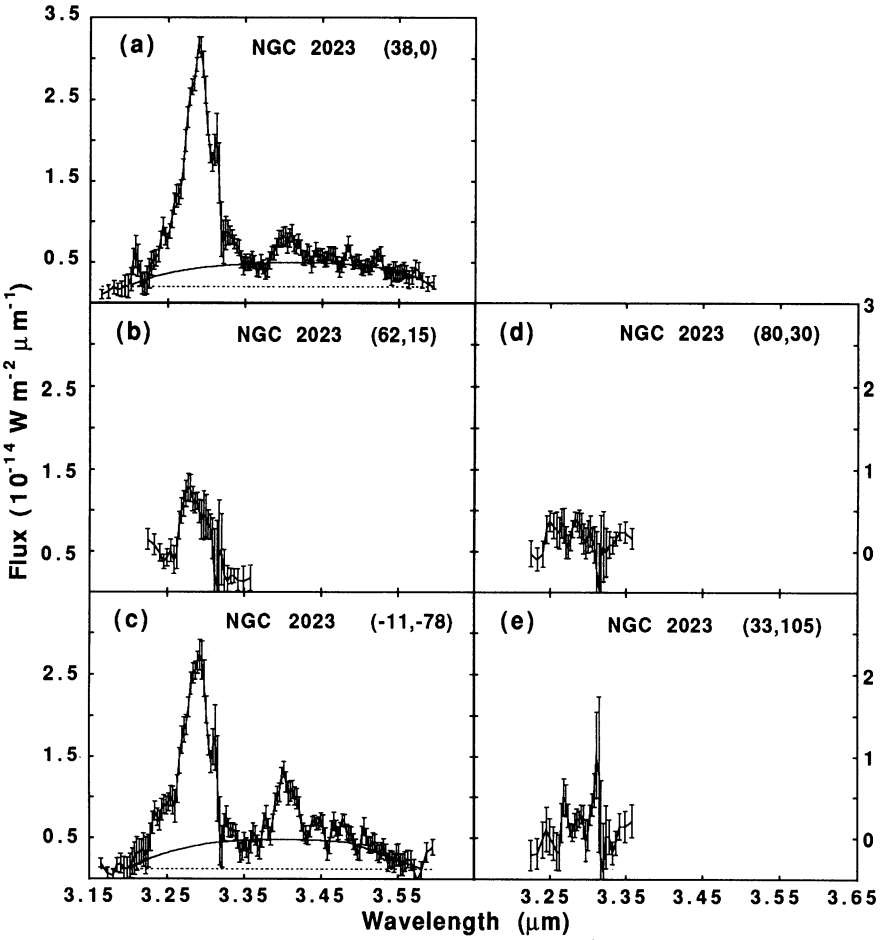

FIG. 4.—The 3.15–3.6 μm spectra measured at different positions within the reflection nebula NGC 2023. The letters *a–e* correspond to the positions shown in Fig. 2 and are ordered by increasing distance from the star, HD 37903. In this nebula, the observed positions were chosen along the bright red filaments mapped by Witt & Malin (1989). Only positions *a* and *c* were bright enough in this spectral region to permit detection of the 3.29 and 3.4 μm features and the underlying plateau. As in Fig. 3, the plateau is arbitrary defined by the solid line, with the dotted line taken as the continuum.

spectrum has been modeled using the spectrum from Kurucz (1979) for a 13,000 K star with $g = 4.0$. We have determined the UV flux intensity at the different observed positions by taking acount of the projected distances. These values are listed under "G" in Table 2. A value of 1″ has been used to estimate the average G value at the stellar position.

There is no direct measurement of the hydrogen density in this object. However, the H_2 $v = 1 \rightarrow 0$ $S(1)$ emission line is observed to be localized in a shell which is 0.01 pc thick. Theoretical studies (Tielens & Hollenbach 1985) predict that this corresponds to a variation in visual extinction of $\Delta A_V \sim 1$, which corresponds to a total hydrogen column density of $\Delta N_H \sim 2 \times 10^{21}$ cm^{-2}. The density is then estimated to be $n_H \sim 5 \times 10^4$ cm^{-3}. In view of the lack of further studies of this region, we assume that the local extinction is negligible for the observed positions.

3.2.2. *NGC 2023*

This reflection nebula, at 480 pc from Earth, is illuminated by HD 37903 of spectral type B1.5V and luminosity $L \sim 2.9 \times 10^4$ $L_\odot$ (Howe et al. 1991, and references therein). The G values for this object (Table 2) have been determined from the projected distances using the spectrum of Kurucz (1979) for a star of $T = 22{,}500$ K and $g = 4.0$. Gatley et al. (1987) have studied this region both in the $v = 1 \rightarrow 0$ $S(1)$ H_2 line and in the $J = 1 \rightarrow 0$ ^{12}CO line emission. The H_2 emission is localized in thin filaments which give the appearance of resulting from limb brightening of shell-like structures (Gatley et al. 1987; Field et al. 1994). From the observed vibrational line ratios of H_2, Burton, Hollenbach, & Tielens (1990) have determined a density of $n_H \simeq 10^5$ cm^{-3} for the position 80″ south in projection from the star. High-level CO lines (Jaffe et al. 1990), and [O I] and [C II] atomic fine-structure lines (Steiman-Cameron et al. 1995) confirm the presence of high-density clumps ($\sim 10^5$ cm^{-3}) embedded in lower density interclump gas ($\sim 10^3$ cm^{-3}). As in the case of NGC 1333, the G values of the UV field in NGC 2023 (Table 2) have been estimated by taking into account only the projected distances, since local extinction and geometry are difficult to quantify.

3.2.3. *The Orion Bar and the Red Rectangle*

For the Orion Bar, most of the UV light comes from the Trapezium stars, Tielens et al. (1993) have determined that $G = 5 \times 10^4 G_o$ at position 4 and that the density is $n_H = 5 \times 10^4$ cm^{-3}. The same authors have made a detailed study of the emission from the photodissociation region (PDR). They found that the maximum of the H_2 emission occurs at a visual extinction $A_V = 2$ in the PDR, while that for the CO emission occurs for $A_V \geq 4$, in agreement with theoretical models of these regions (Tielens & Hollenbach 1985). Using these results

TABLE 2

PEAK INTENSITIES OF THE EMISSION FEATURES IN THE 3 μm REGION WITHIN SEVERAL NEBULAE

Position	F/C[a]	$I_{plateau}$[b]	$I_{3.29\,\mu m}$[b]	$I_{3.40\,\mu m}$[b]	$\frac{I_{3.40\,\mu m}}{I_{3.29\,\mu m}}$	$G(G_o)$[c]
NGC 1333[d]						
(0, 0)	0.6	1.27	7.8	1.10	0.14	4.8×10^5
(2, −5)	11	1.03	9.9	1.44	0.15	1.6×10^4
(0, −9)	17	1.13	10.4	1.91	0.18	5.9×10^3
(−6, −11)	37	1.62	10.0	2.75	0.27	3.1×10^3
(0, −13)	24	1.42	10.5	2.87	0.27	2.8×10^3
(−11, −11)	25	1.11	6.3	1.56	0.25	2.0×10^3
NGC 2023[d]						
(38, 0)	14	0.30	2.8	0.36	0.13	5.2×10^4
(62, 15)	2.5	...	0.8	...	...	1.8×10^4
(−11, −78)	20	0.36	2.4	0.81	0.34	1.2×10^4
(80, 30)	...	0.4	...	...	...	1.0×10^4
(33, 105)	...	0.4	...	...	...	6.2×10^3
Orion Bar[e]						
P4	19	2.9	39	5.0	0.13	5.0×10^4
10″ S	27	2.4	20	3.5	0.17	7.1×10^3
20″ S	34	0.64	5.0	1.3	0.26	1.7×10^2
Red Rectangle[e]						
HD 44179	0.7	...	1600	100	0.06	1.5×10^6
HD 44179 5″ N	3	...	45	6	0.13	5.9×10^4

[a] Ratio of the 3.29 μm feature to the adjacent continuum.

[b] Peak intensities in units of 10^{-14} W m^{-2} μm^{-1}. $I_{plateau}$ is the intensity of the plateau defined underneath the features (see Figs. 3 and 4 and Geballe et al. 1989). The peak intensities of the 3.29 and 3.40 μm features are measured above this plateau.

[c] Intensity of the UV radiation field, G, in units of $G_o = 1.6 \times 10^{-3}$ ergs cm^{-2} s^{-1} determined as described in § 3.2.

[d] Spectra displayed in Figs. 3 (NGC 1333) and 4 (NGC 2023). Positions are given by their offsets in arcseconds from the central star, SVS3 for NGC 1333 and HD 37903 for NGC 2023.

[e] From Geballe et al. 1989.

and the H_2 and CO map shown in Tielens et al. (1993), we have estimated an A_V of about 1 and 3 at 10″S and 20″S of position 4, respectively. The UV extinction is assumed to be given by exp $(-1.8A_V)$, according to Tielens & Hollenbach (1985).

In the case of the Red Rectangle located at 330 pc from the Earth, the illuminating star HD 44179 is of spectral type A0 with $T = 10{,}000$ K and $L = 10^3\ L_\odot$ (Cohen et al. 1975). We have modeled the HD 44179 spectrum using the spectrum from Kurucz (1979) for a 10,000 K star with $g = 4.0$. The spectrum at the (0, 0) position is assumed to correspond to emission at 1″ from the star (Geballe et al. 1989).

3.3. *Variation of the* 3.29 *and* 3.40 μm *Band Intensities with G*

In Figure 5, the peak intensity of the 3.29 μm band and the ratio of the intensities of the 3.40 to the 3.29 μm bands are plotted as a function of the intensity of the UV radiation field, G. As expected, the 3.29 μm band intensity clearly increases with increasing values of G in the case of the Orion Bar and of the Red Rectangle. For NGC 1333 and NGC 2023, the data points show a lot of dispersion, which indicates that either the estimation of the UV field (Table 2) is not correct or other factors are important as well (e.g., density variations and geometry).

In contrast, the 3.40 to 3.29 μm band intensity ratio (hereafter 3.40/3.29 μm ratio) shows a better correlation with G. This is almost certainly because the factors which equally affect the intensities of both bands (e.g., column density of molecules) cancel out in the intensity ratio. The 3.40/3.29 μm ratio tends to decrease logarithmically with G.

The dependence is best established for the Orion Bar region. A variety of observations have shown that the Bar is an edge-on, limb-brightened photodissociation region illuminated by the Trapezium star, Θ^1 Ori C, from the northwest (see Tielens et al. 1993). The dust attenuation of the radiation field in the PDR (i.e., distance from position 4) is well traced by various molecular lines. Most of the variation in G in this nebula reflects this attenuation by dust. The geometry and structure of the other regions are not as well determined. However, in all cases the IR emission bands as well as other molecular emissions tend to show some filamentary structure which is similar to that in the Orion Bar. This indicates that we can treat these as limb-brightened structures in the plane of the sky. In HD 44179 and for some of the positions in NGC 1333, the decrease in G appears to solely reflect the effects of geometric diluation. The trends in these data parallel the data for the Orion Bar in which extinction does dominate the variations in G. Hence, we believe that this variation of the 3.40/3.29 μm ratio with G is not an artifact introduced by uncertain extinction effects, but reflects an intrinsic property of the emitting species in a changing radiation field. Following Geballe et al. (1989), we attribute this variation to the photochemical evolution of PAHs under the influence of strong UV radiation fields.

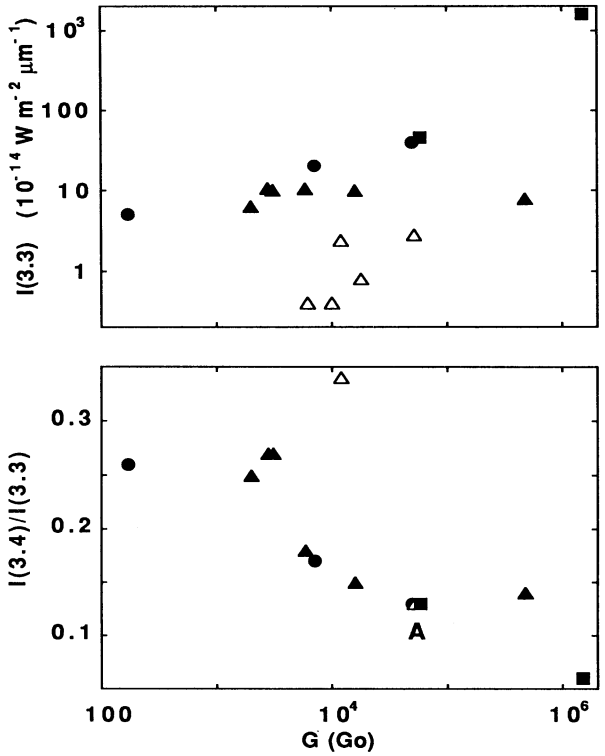

FIG. 5.—Peak intensity of the 3.29 μm band (*top*) and the ratio of the peak intensities of the 3.40 μm band to the 3.29 μm band (*bottom*) as a function of the intensity of the UV radiation field, *G* (see Table 2). The filled and open triangles represent different spatial positions within the reflection nebulae NGC 1333 SVS3 and NGC 2023, respectively (this work). Dots and squares correspond to positions in the Orion Bar photodissociation region and in the Red Rectangle reflection nebula, respectively (Geballe et al. 1989). The letter *A* indicates the position of an open triangle, square, and dot which are very close.

4. METHYL SIDE GROUPS AND THE 3.40 μm BAND

The 3.29 μm emission band is generally identified as the CH stretching mode of free-flying polycyclic aromatic hydrocarbons, PAHs (Léger & Puget 1984; Allamandola, Tielens, & Barker 1985). Other models propose that the carriers of this feature are associated with dust grains (Duley & Williams 1981; Sakata et al. 1984, 1987; Borghesi, Bussoletti, & Colangeli 1987; Papoular et al. 1989). In the case of emission by a solid, the bands are expected to sit on the top of a continuum. The highest values (25–37) measured in NGC 1333 for the feature-to-continuum ratio at 3.3 μm seem to be difficult to reconcile with the solid-state models which would tend to favor lower values than for gas-phase PAHs. Guillois et al. (1994) reported that this ratio ranges from 10 to 25 in the case of coal grains, for which the continuum is particularly low as a result of the semiconductor properties of these grains. Although more observational constraints are still required, the case of NGC 1333 seems to favor free-flying PAH molecules as the carriers of the 3.29 μm emission feature. This issue is discussed in detail by Puget, Léger, & d'Hendecourt (1995) and Papoular et al. (1995). In the following, we discuss the origin of the 3.40 μm emission band as caused by PAH molecules.

Emission near 3.40 μm can arise from the aliphatic CH stretch of methyl ($-CH_3$) or methylene ($-CH_2$) side groups, hot band emission ($v = 2$–1 transition) from the aromatic C-H stretch, and overtone and combination bands involving the C-C stretching and/or C-H bending modes (Allamandola et al. 1989). While hot band emission near 3.4 μm is required by the PAH hypothesis (Barker et al. 1987), Jourdain de Murizon et al. (1990b) stressed that emission at 3.40 μm could arise from aliphatic side groups attached to the periphery of the PAH molecules. Although it is likely that all the above contribute to the emission structure observed in the 3.2–3.6 μm region, there is now evidence that the 3.40 μm band in methyl ($-CH_3$) side groups on PAHs is the dominant contributor to the 3.40 μm feature.

Recent observations tend to argue against identifying the 3.40 μm band with the $v = 2$–1 hot band transition of the C-H aromatic mode alone. As this study shows, the observed 3.40/3.29 μm ratio can be as large as ~0.3. Considering that the 3.40 μm band is about 1.5 times narrower than the 3.29 μm band, then the 3.40/3.29 μm integrated intensity ratio is measured to be as large as ~0.2. Such high levels of excitation lead to rapid dissociation of the C-H bond before IR emission can occur. The observed ratio of 0.2 implies that the carrier is smaller than benzene (C_6H_6), which is untenable in terms of hot band emission (Schutte, Tielens, & Allamandola 1993). Indeed, Schutte et al. calculated that the highest possible 2–1/1–0 integrated intensity ratio would range from 0.17 for benzene (C_6H_6) to 0.11 for coronene ($C_{24}H_{12}$) before photodissociation dominates IR emission. An additional argument against identifying the 3.40 μm band with hot band emission is the recent observation of the 2–0 overtone at 1.68 μm toward the planetary nebula IRAS 21282+5050 (Geballe et al. 1994). The position of the $v = 1$–0 transition being 3.294 μm in that object, the $v = 2$–1 transition is then expected to occur at about 3.43 μm and not at 3.40 μm. The observed intensity of the 2–0 band can be used to predict the 2–1 intensity using the experimentally measured Einstein *A*-values of these transitions. The calculated $v = 2$–1 intensity is only 11% of the 3.40 μm band intensity in this source. Thus, we conclude that most of the intensity in the 3.40 μm satellite band cannot be the result of hot band emission. Hot band emission could contribute to the shoulder which is observed on the long-wavelength side of the 3.40 μm band in the spectrum of IRAS 21282+5050 (Jourdain de Muizon et al. 1990a, b). This shoulder generally seems to be present in spectra taken at positions close to the exciting star: for example, at Position 4 in Orion, and for position (0, −9) in NGC 1333.

While emission from aliphatic side groups attached to PAHs, as put forward by Jourdain de Muizon et al. (1990b) provides an attractive alternative to account for the 3.40/3.29 μm ratio, previous comparisons with laboratory spectra were not very favorable (d'Hendecourt & Léger 1987; Jourdain de Muizon et al. 1990b; Sandford 1991; Schutte et al. 1993). However, until recently, most of the IR spectral data available were for PAHs dissolved in mineral oil mulls or suspended as crystallites in salt pellets, whereas in the emission zones, individual PAHs are expected to be in the gas phase (Léger & Puget 1984; Allamandola et al. 1985). The suspensions perturb the individual molecules, resulting in spectral shifts and band intensity alterations.

Recently, spectra of gas-phase PAHs with and without side groups have been measured (Joblin 1992; Joblin, d'Hendecourt, & Léger 1995b) and have confirmed that the earlier solid-state spectra reflected matrix interactions, which shifted and enhanced various spectral features. Contrary to the earlier comparisons, the gas-phase spectra of methylated PAHs give a good agreement in peak position and width with the interstellar 3.40 μm band. This is illustrated by Figure 6,

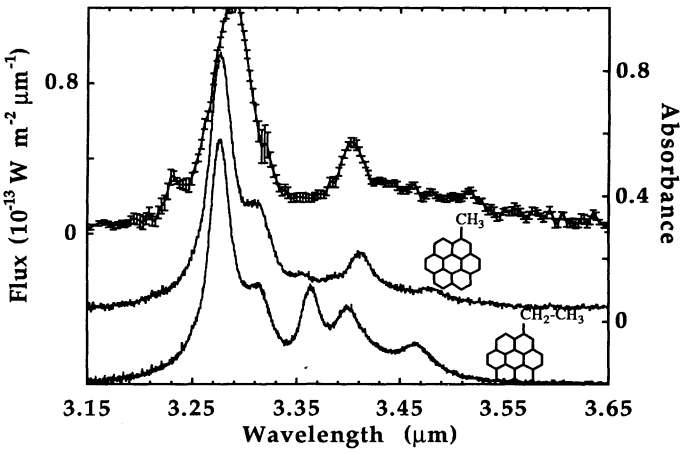

FIG. 6.—The 3.15–3.65 μm spectrum of NGC 1333 (*top*), at 13″S from the star SVS3, compared with the gas-phase spectra of methyl-coronene ($C_{24}H_{11}-CH_3$) and ethyl-coronene ($C_{24}H_{11}-C_2H_5$) at 450 C (laboratory data taken from Joblin et al. 1995b; Joblin 1992). The relative integrated intensity of the 3.4 and 3.3 μm bands of methyl-coronene after subtraction of a plateau is 0.11.

where the absorption spectrum of methyl-coronene in the gas phase is compared with the spectrum of NGC 1333 (0, −13) (Fig. 3*e*). Laboratory measurements show that the position of the 3.3 μm band of PAHs shifts to longer wavelengths when the vibrational temperature of the molecules increases (Joblin et al. 1995a). It is not surprising then that the 3.3 μm band of methyl-coronene which is measured at 720 K in the laboratory is blueshifted compared with the interstellar band which corresponds to emission temperatures of about 1200 K (see Joblin et al. 1995a for more details). The 3.4 μm band of methyl-coronene is less sensitive to temperature variations. It occurs at 3.41 μm, slightly redshifted compared with the interstellar band, but it still gives the best fit, with a laboratory measured spectrum, ever obtained for this band. Longer aliphatic chain side groups, like $-CH_2CH_3$, produce a band at 3.36 μm (see Fig. 6; Joblin 1992; Joblin et al. 1995b) which is not observed in the studied regions. Comparing the integrated band intensities of methyl-coronene (Fig. 6) with the observed 3.29 and 3.40 μm feature intensities, we can estimate that PAHs emitting in the 3 μm range at position (0, −13) contain about one $-CH_3$ side group for eight aromatic C-H bonds (for consistency with the observations, the band intensities in the case of methyl-coronene have been measured underneath a plateau).

5. PHOTOCHEMICAL EVOLUTION OF "METHYLATED" INTERSTELLAR PAHs

If the 3.40 μm band is attributable to methylated PAHs, the question is now whether the observed variations of the 3.40/3.29 μm ratio could be accounted for by these molecules. In the following, a model of the evolution of methylated PAHs resulting from variations in the intensity of the UV field is discussed.

If sufficiently excited, a PAH can lose its energy through unimolecular decomposition much more rapidly than through IR emission. This can result in the loss of a peripheral —H atom or $-CH_3$ side group. The balance between unimolecular decomposition and IR emission has been discussed by Tielens et al. (1987) and Allamandola et al. (1989). The reactions involved are

$$\mathrm{PAH} + h\nu \rightarrow \mathrm{PAH}^* + \mathrm{H} \quad k_1, E_1 = 4.85\ \mathrm{eV}, \tag{1}$$

$$\mathrm{PAH}^* + \mathrm{H} \rightarrow \mathrm{PAH} \quad k_2, \tag{2}$$

where PAH* signifies a dehydrogenated PAH, k_i is the reaction rate, and E_i is the activation energy. In the following, we will use the same procedure, adapted to include the photochemical evolution of the methyl side groups through equations (3)–(6):

$$\mathrm{PAH} - \mathrm{CH_3} + h\nu \rightarrow \mathrm{PAH} = \mathrm{CH_2} + \mathrm{H} \quad k_3, E_3 = 3.7\ \mathrm{eV}, \tag{3}$$

$$\mathrm{PAH} = \mathrm{CH_2} + \mathrm{H} \rightarrow \mathrm{PAH} - \mathrm{CH_3} \quad k_4, \tag{4}$$

$$\mathrm{PAH} - \mathrm{CH_3} + h\nu \rightarrow \mathrm{PAH}^* + \mathrm{CH_3} \quad k_5, E_5 = 4.0\ \mathrm{eV}, \tag{5}$$

$$\mathrm{PAH} = \mathrm{CH_2} + h\nu \rightarrow \mathrm{PAH}^* + \mathrm{CH_2} \quad k_6, E_6 = 4.9\ \mathrm{eV}, \tag{6}$$

where PAH = CH_2 indicates the =CH_2 group attached to a PAH. One can view the activation energy or energy barrier as the energy which must be localized in a given bond, long enough for the dissociation to take place. The probability for such a localization depends on the size of the molecule. Rather than using RRKM theory, we have calculated the unimolecular dissociation rate of a PAH using the inverse Laplace transform approximation:

$$k(E) = A_i \frac{\rho(E - E_i)}{\rho(E)}, \tag{7}$$

where A_i and E_i are the Arrhenius parameters in the high-pressure limit, and $\rho(E)$ is the density of states at an internal energy E (Forst 1973). The density of states for PAHs is given in Tielens (1993). For A_i, we adopt a value of 3×10^{16} s^{-1}, appropriate for H loss by benzene (see Allamandola et al. 1989).

The dissociation rates of different bonds with respect to the aromatic network are plotted in Figure 7 as a function of molecular size. An internal energy of 10 eV was adopted, which is the average energy of the UV photons absorbed by PAHs. The actual probability of dissociation depends on the competition with other deexcitation channels. The IR relaxation rate, which is the other major energy loss channel, is also indicated in Figure 7. When the dissociation rate exceeds the IR emission rate, unimolecular decomposition occurs. Over a certain critical size, IR emission dominates. Thus, photodissociation is important only for the smaller species.

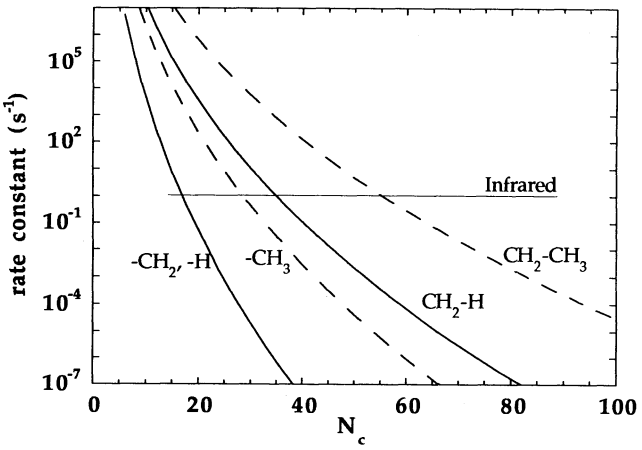

FIG. 7.—Dissociation rates of different bonds within aliphatic subgroups attached to the periphery of PAHs as a function of molecular size (N_C: number of C atoms). Details of the calculations are given in § 5 of the text. A value of 4.85 eV has been used for the aromatic C-H bond dissociation (Kiefer et al. 1985). The other values have been taken from Table 2 in Geballe et al. (1989). The horizontal line represents the relaxation rate by IR emission.

The populations of $-CH_3$ and $=CH_2$ side groups, $n(CH_3)$ and $n(CH_2)$ respectively, are given by the following equations:

$$\frac{dn(CH_2)}{dt} = n(CH_3)k_{UV}p_3 - k_4 n(CH_2)n_H - n(CH_2)k_{UV}p_6 , \quad (8)$$

$$\frac{dn(CH_3)}{dt} = -n(CH_3)k_{UV}p_3 + k_4 n(CH_2)n_H - n(CH_3)k_{UV}p_5 . \quad (9)$$

We adopt 10^{-9} cm^3 s^{-1} for k_4 and k_2 (Tielens et al. 1987). The UV absorption rate, k_{UV}, is $k_{UV} = 7 \times 10^{-10} N_C\, G$ s^{-1} for a molecule containing N_C carbon atoms and submitted to the UV field G; p_3 is the probability of H loss from the methyl side group for a vibrationally excited PAH: $p_3 = k_3/(k_3 + k_5 + k_1 + k_{IR})$, where k_i are the unimolecular decomposition rates shown in Figure 7 and associated to equation i, k_{IR} is the IR radiative relaxation rate, and we have neglected all other energy loss channels. The dissociation probabilities p_5 and p_6 are calculated in a similar way: $p_5 = k_5/(k_3 + k_5 + k_1 + k_{IR})$ and $p_6 = k_6/(k_6 + k_1 + k_{IR})$. The probabilites p_5 and p_6 are always smaller than p_3, with p_3/p_5 and $p_3/p_6 > 15$ for $N_C \geq 20$ (see Fig. 7). When the molecular size decreases from 20 C atoms to smaller sizes, p_6 becomes on the order of p_3. For larger sizes, the populations of $-CH_3$ and $=CH_2$ side groups are well approximated by the equilibrium:

$$\frac{n(CH_3)}{n(CH_2)} = \frac{k_4 n_H}{k_{UV} p_3} . \quad (10)$$

The decay of side groups with time is dominated by reaction (5) as $p_5 \gg p_6$ for $N_C > 20$. Reactions (5) and (6) are essentially irreversible in the interstellar medium, since the gas phase abundance of C atoms and CH_n groups is very small compared with that of H. The decay of side groups is then given by

$$\frac{dn(CH_3)}{dt} = -n(CH_3)k_{UV}p_5 . \quad (11)$$

Hence, over time, the number of $-CH_3$ groups will decrease, and so will the 3.40 μm band. Given the reaction rates and activation energies involved, this will occur on a timescale governed by the local radiation field. Adopting a typical evolutionary timescale of 10^5 yr for the regions under consideration, we can determine the minimum size of the interstellar PAHs which still have their side groups as a function of the radiation field G. We define the critical size, $N_{crit}(-CH_3)$, as the size for which PAHs have lost half their side groups over this evolutionary timescale. The variation of this critical size with the radiation field is reported in Table 3.

In a similar vein, we can evaluate the critical PAH size for aromatic H loss (reactions [1] and [2]) as a function of G. The fraction of dehydrogenated PAHs is given by

$$f(-H) \equiv \frac{n(PAH^*)}{n(PAH)} = \frac{k_1}{k_2 n_H} = \frac{0.7 G N_C p_1}{n_H} . \quad (12)$$

Adopting an H-density of $n_H = 5 \times 10^4$ cm^{-3}, we have evaluated this expression for various UV fields as a function of N_C. The results (Fig. 8) show that PAHs containing more than about 25 C atoms will be fully hydrogenated [$f(-H) < 0.1$] for all reasonable UV fields [see $N_{crit}(-H)$ in Table 3]. The fraction of dehydrogenated PAHs increases with decreasing PAH size (Fig. 8). The dehydrogenated fraction levels off at small sizes when every photon absorbed leads to H loss [$f(-H) = 1$] rather than IR relaxation. The small decrease in $f(-H)$ for even smaller N_C results from the drop-off in UV absorption cross section with size.

TABLE 3

CRITICAL PAH SIZE FOR BOND PHOTODISSOCIATION AS A FUNCTION OF THE UV FIELD G

(G_o)	$N_{crit}(-CH_3)$ (C atoms)	$N_{crit}(-H)$ (C atoms)
10^6	102	24
10^5	93	20
5×10^4	90	18
10^4	85	16
5×10^3	82	...
10^3	77	...
10^2	69	...
10	62	...
1	55	...

NOTES.—In this calculation, we assumed $n_H = 5 \times 10^4$ cm^{-3}. The calculated $N_{crit}(-H)$ depends on n_H (as G/n_H), but $N_{crit}(-CH_3)$ does not depend on n_H as long as the equilibrium given by eq. (10) is satisfied.

It is interesting to see how the photochemistry involving aromatic $-H$ and $-CH_3$ side groups will affect the 3.40/3.29 μm ratio. All PAHs with $N > N_{crit}(-H)$ will contribute to the 3.29 μm band, whereas only molecules with $N > N_{crit}(-CH_3)$ will contribute to the 3.40 μm band. The flux emitted at 3.29 μm as a function of the PAH size has been modeled by Schutte et al. (1993). Here we consider a size distribution containing PAHs (methylated PAHs) between 20 and 130 C atoms. Smaller molecules are not considered, as our modeling of side group photodissociation requires $N_C > 20$. Molecules containing more than 130 C atoms are not considered, as they do not get excited enough in these fields to contribute significantly to the 3.29 μm band intensity. Implicit in this calculation is that the 3.29 and 3.40 μm bands follow the same emission law. This is reasonable, as both bands originate from levels at similar energies above the ground state and are likely carried by similar molecules.

The results of this integration are shown in Figure 9. The calculated curve has been scaled by a factor of 2, which corre-

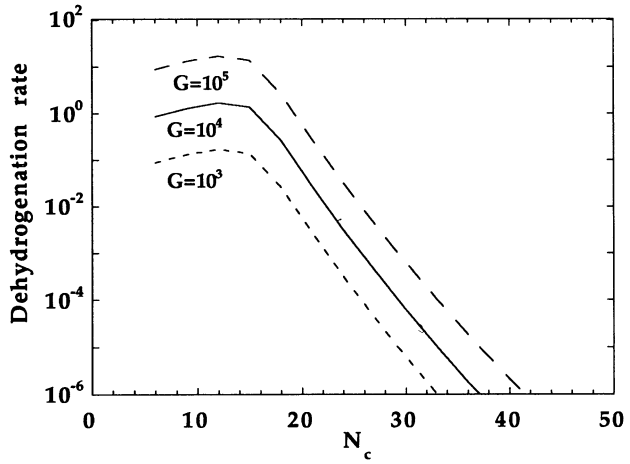

FIG. 8.—Dehydrogenation rate of interstellar PAHs as a function of the molecular size and for different values of the UV radiation field intensity, G (in units of G_o). The assumed H density is $n_H = 5 \times 10^4$ cm^{-3}. The dehydrogenation rate is found to be negligible for all PAHs containing more than about 25 C atoms.

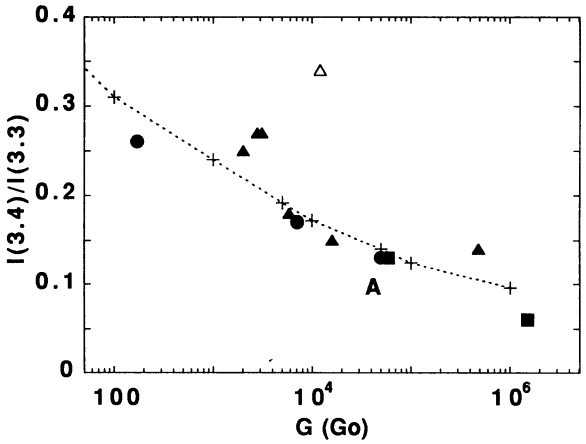

FIG. 9.—Comparison of the photochemical model described here (*crosses connected by dotted line*) with the observed 3.4/3.3 μm intensity ratio (Fig. 5). The decrease of this ratio with G is interpreted in terms of the loss of methyl side groups attached to the periphery of PAHs.

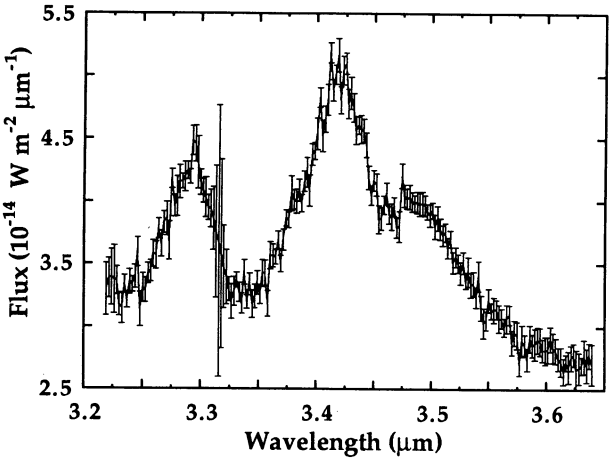

FIG. 10.—The 3 μm spectrum of IRAS 05341+0852 measured at a resolution of 0.006 μm.

sponds to an initial $-CH_3/-H$ ratio of 1 if using the band strengths measured for methyl-coronene.

6. DISCUSSION

The photochemical model described above explains both the trend and the magnitude of the observed 3.40/3.29 μm ratio variations reasonably well. Only one point in NGC 2023 (*open triangle*) seems to behave differently, but this could be related to the complexity of this region (Field et al. 1994), which complicates the quantification of the UV field.

A recent study suggests that the internal energy required for aromatic H loss is only 2.8 eV (Jochims et al. 1994) rather than the 4.85 eV measured in high-pressure studies of benzene (Kiefer et al. 1985) and adopted here. This low energy is actually less than the energies for loss of methyl or ethyl side groups used in this work. This is at odds with experimental data on aromatic systems, which show methyl and ethyl side group loss before aromatic H loss (Benson 1965; Stein, Golden, & Benson 1977; Bruinsma et al. 1988). Here we emphasize that our main conclusion that the 3.40/3.29 μm ratio variations result from photochemically driven loss of CH_3 versus H only requires that the CH_3 loss barrier is less than that of H. Variations in the adopted energies will affect the critical sizes involved in these processes but not the trend shown in Figure 9.

Combined with the spectral agreement shown in Figure 6, this model strongly supports the presence of methyl side groups at the periphery of interstellar PAHs, as suggested by Jourdain de Muizon et al. (1990b). Our model predicts that the 3.40/3.29 μm ratio can be as large as 2 in regions protected from photodissociation processes.

Images at 3.3 and 3.4 μm of the M17 photodissociation region indicate that the two bands have comparable intensities in the most distant regions from the exciting star (Giard, Bernard, & Dennefeld 1992), although the lack of a 3 μm spectrum in this region prevents confirmation. Geballe & van der Veen (1990) have measured the 3 μm spectrum of the proto–planetary nebula IRAS 05341+0852 (with an F-type central star), in which the 3.3 and 3.4 μm emission bands do have comparable intensities (a value of 1 for the peak intensity ratio). A few other examples are also known (Geballe et al. 1992). Recently an improved spectrum of IRAS 05341+0852 was obtained by us at UKIRT, using CGS4, on 1994 April 16; it is shown in Figure 10. The prominent 3.4 μm band peaks at 3.419 ± 0.001 μm. This band is cleary redshifted and broader compared with the 3.40 μm band observed in reflection nebulae (Fig. 11). It shows more similarity with the strong 3.4 μm absorption band which is characteristic of the diffuse interstellar medium and attributed to the CH stretch in aliphatic hydrocarbons (Pendleton et al. 1994; Ehrenfreund et al. 1991; Sandford et al. 1991). The absence of a significant feature at 3.38 μm indicates that the $-CH_2/-CH_3$ ratio is much larger in the case of IRAS 05341+0852 than in the diffuse interstellar medium. This is achieved for long chains or cyclic aliphatic hydrocarbons (for example, cyclohexane C_6H_{12}; laboratory spectra from d'Hendecourt & Allamandola 1986).

In the case of the diffuse interstellar medium, it is very likely that the aliphatic chains are part of grains (Sandford et al. 1991; Ehrenfreund et al. 1991). On the other hand, in the more benign environment of proto–planetary nebulae, fragile species such as aliphatic hydrocarbon chains, which are produced in the outflow, could be present as gaseous species. However, as these molecular chains are easily dissociated upon UV irradiation, they are expected to disappear during the planetary nebula stage when the central source emits strongly in the UV. As an example, Figure 11 compares the 3.4 μm spectrum of the planetary nebula IRAS 21282+5050 (Jourdain de Muizon et al. 1990a) with the spectra of the proto–planetary nebula IRAS 05341+0852, and of the reflection nebula NGC 1333. The planetary nebula spectrum exhibits the 3.40 μm band and a shoulder at about 3.43 μm. Although a contribution to this shoulder could arise from the hot band of the 3.3 μm feature (Geballe et al. 1994), there is likely a contribution of the strong 3.42 μm band observed in IRAS 05341+0852 and attributed to aliphatic chains. This contribution is expected to disappear for longer evolution times, provided that there is no replenishment of this aliphatic compound, for example from grain evaporation. The case of NGC 7027, which is an evolved planetary nebula, seems to support this assumption. Indeed, the 3.40 μm feature in this object does not have a strong shoulder (Lowe et al. 1991) and looks similar to the band observed in reflection nebulae. We note that a shoulder at about 3.43 μm is also observed at position 4 in the Orion Bar and at position (0, −9) in NGC 1333. In these two cases, it is more likely that this shoulder arises from hot band emission. It is clear that this

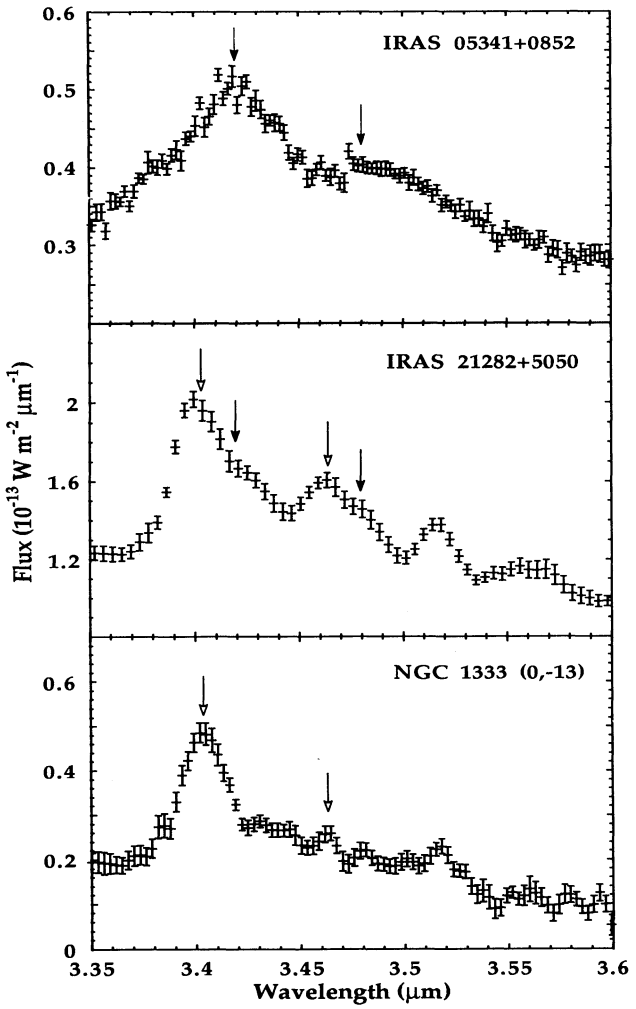

FIG. 11.—Comparison of the 3.4 μm emission features observed in the proto-planetary nebula IRAS 05341+0852, the planetary nebula IRAS 21282+5050, and the reflection nebula NGC 1333 at 13″S from the star SVS3. As discussed in the text, the spectrum of IRAS 21282+5050 may result from a contribution of the bands observed in IRAS 05341+0852 (*filled arrows*) and those observed in NGC 1333 (*open arrows*).

spectral region is very complex, with many different components contributing. A concerted study of a large number of different objects in this wavelength region is required to disentangle these different components and make their assignment.

We propose the following evolution: the initial mixture of gas-phase aromatic and aliphatic compounds is submitted to the interstellar UV field. This leads to photodissociation of the less photostable aliphatic chains. If these chains are attached to aromatic structures, then the most likely photodissociation products are $=CH_2$ groups attached to the aromatic skeleton, which, when subjected to reaction (4), will rapidly lead to a high abundance of CH_3 side groups at the periphery of aromatic molecules. The value of about 2 predicted in § 5 for the initial 3.40 over 3.29 μm peak intensity ratio indeed neglects the presence of longer chains. The diffuse interstellar medium (ISM) with a UV field intensity of $G = 1G_o$, seems to give a simple and optimum case in which $-CH_3$ side groups can reasonably survive and longer chains are expected to be photodissociated. Using the dissociation rates of Figure 7, the critical size for the dissociation of $-CH_3$ side groups is estimated to be 55 C atoms, whereas it is 112 C atoms for longer chains, like $-CH_2-CH_3$. We estimate that in the diffuse medium, the 3.40 over 3.29 μm peak intensity ratio is 0.5. This implies a value of 0.33 for the ratio of the integrated intensities, considering that the 3.40 μm band is about 1.5 narrower than the 3.29 μm band in NGC 1333. Using the band intensities of methylcoronene and assuming that the $-CH_3/-H$ ratio is independent of the PAH size, a proportion of about one $-CH_3$ side group for four peripheral hydrogens is derived. Recently, Bernard et al. (1994) have shown that the emission of the diffuse ISM observed in the *COBE* 3.5 μm broad ($\Delta\lambda = 1$ μm) band is much stronger than expected on the basis of the 3.3 μm narrow ($\Delta\lambda = 0.16$ μm) band AROME measurements. This indicates the presence of other emission component(s) in the 3 μm region besides the 3.3 μm feature. Here we suggest that there is an important contribution to the emission measured in the 3.5 μm *COBE* band from aliphatic sidegroups on interstellar PAHs. This can be checked in the near future using the data from the Infrared Telescope in Space mission or the Infrared Space Observatory (ISO) satellite.

The existence of $-CH_3$ side groups requires the presence of a band at about 6.9 μm associated with the bending mode of this group. A band at 6.9 μm has indeed been identified as part of the IR emission band family by Cohen et al. (1986). However, it could be associated with C-C stretching modes of PAHs with specific structures (Allamandola et al. 1989). Careful spatial correlation studies of the 3.4 and 6.9 μm band intensities are then required as a test of the presence of aliphatic side groups. Such observations have been planned using the IR satellite ISO.

The detection of $=CH_2$ side groups would provide direct confirmation of the importance of photochemical evolution of PAHs. However, the abundance of such groups is predicted to be very small. The abundance of $=CH_2$ side groups at $t = 10^5$ yr can be estimated from

$$\frac{n(CH_2;\, t=10^5)}{n(CH_3;\, t=0)} = \frac{n(CH_2;\, t=10^5)}{n(CH_3;\, t=10^5)} \frac{n(CH_3;\, t=10^5)}{n(CH_3;\, t=0)}, \quad (13)$$

where the first and second fraction on the right side are given by equations (10) and (11). The results are shown in Figure 12. For sizes much less than the critical size, the second factor in

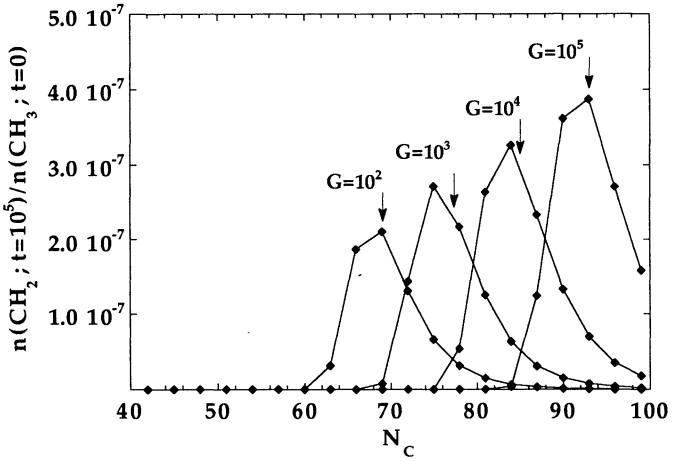

FIG. 12.—Relative abundance as a function of molecular size of $=CH_2$ side groups compared with $-CH_3$ side groups, for a typical timescale of 10^5 yr, and for different values of the UV radiation field intensity, G. These results suppose that the populations of $=CH_2$ and $-CH_3$ side groups are at equilibrium (eq. [10]) and that $n_H = 5 \times 10^4$ cm^{-3}. The arrows indicate the values of $N_{crit}(-CH_3)$ associated with each UV field (Table 3). This critical size represents the size for which PAHs have lost half their $-CH_3$ side groups over the evolutionary timescale. Much smaller PAHs have lost all their side groups, and much larger PAHs are not subjected to photodissociation.

equation (13) drives the abundance of $=CH_2$ groups down. Essentially, such small PAHs have no aliphatic side groups. PAHs much larger than $N_{crit}(-CH_3)$ do not evolve photochemically and hence have no $=CH_2$ side groups. Evaluating equation (13) at the critical size (~ 80) and for a typical value of the UV field, $G = 10^4 G_o$, we find

$$\frac{n(CH_2; t = 10^5)}{n(CH_3; t = 10^5)} \sim 3 \times 10^{-7} . \quad (14)$$

Besides these abundance problems, detection of the $=CH_2$ mode may also be hampered by its closeness in wavelength to the aromatic CH stretch (Lutoshkin, Kotorlenko, & Krugylak 1972).

Finally, the weak satellite bands at 3.46 μm and 3.52 may also result from (other types of) side groups. There is presently no evidence for the candidates ($-OH$, $-NH_2$) considered in Geballe et al. (1989). Given the binding energies, we expect $-OH$ side groups to be very rapidly photodissociated. On the other hand, $-NH_2$ side groups are expected to have a photochemistry comparable with that of $-CH_3$ side groups. However, there is presently no evidence of the N-H stretching modes at 2.87 and 2.95 μm (Geballe et al. 1989).

7. CONCLUSION

We have observed the variation of the prominent 3.29 μm and weaker 3.40 μm bands at several positions within the reflection nebulae NGC 1333 and NGC 2023 and have reexamined similar data for the Red Rectangle and the Orion Bar. We have shown that the systematic variations of the intensity of the 3.40 μm band with respect to that of the 3.29 μm band with distance from the exciting star can be modeled in terms of photochemical erosion of the aliphatic $-CH_3$ subgroups present at the periphery of PAHs as a result of the strong far-ultraviolet (FUV) radiation field in these emission regions. Our analysis suggests that, in general, interstellar PAHs are methylated. We expect that the IR spectrum of the diffuse interstellar medium is characterized by a prominent 3.4 μm emission feature, with a peak intensity about half that of the 3.3 μm emission feature. The strong FUV field in the regions generally observed drives a rapid photochemical evolution leading to a replacement of the $-CH_3$ groups on the smallest PAHs by aromatic $-H$ bonds. We also trace the photochemical evolution of hydrocarbons (aliphatic and aromatic) from the proto–planetary nebula through the planetary nebula phase, using the 3 μm emission spectra of these regions.

REFERENCES

Allamandola, L. J., Tielens, A. G. G. M., & Barker, J. R. 1985, ApJ, 290, L25
———. 1989, ApJS, 71, 733
Barker, J., Allamandola, L., & Tielens, A. G. G. M. 1987, ApJ, 315, L61
Benson, S. W. 1965, J. Chem. Educ., 42, 502
Bernard, J. P., Boulanger, F., Désert, F. X., Giard, M., Helou, G., & Puget, J. L. 1994, A&A, 291, L5
Borghesi, A., Bussoletti, E., & Colangeli, L. 1987, ApJ, 314, 422
Bruinsma, O. S. L., Geertsma, R. S., Bank, P., & Moulijn, J. A. 1988, Fuel, 67, 327
Burton, M. G., Hollenbach, D. J., & Tielens, A. G. G. M. 1990, ApJ, 365, 620
Burton, M. G., Moorhouse, A., Brand, P. W. J. L., Roche, P. F., & Geballe, T. R. 1988, in Interstellar Dust: Contributed Papers, ed. A. G. G. M. Tielens & L. J. Allamandola (NASA Conf. Pub. 3036), 87
Cohen, M., et al. 1975, ApJ, 196, 179
Cohen, M., Allamandola, L., Tielens, A. G. G. M., Bregman, J., Simpson, J. P., Witterborn, F. C.,-Wooden, D., & Rank, D. 1986, ApJ, 302, 737
de Muizon, M., Geballe, T. R., d'Hendecourt, L. B., & Baas, F. 1986, ApJ, 306, L105
d'Hendecourt, L. B., & Allamandola, L. J. 1986, A&AS, 64, 453
d'Hendecourt, L., & Léger, A. 1987, in Planetary and Proto-Planetary Nebulae: From IRAS to ISO, ed. A. Preite Martinez (Dordrecht: Reidel), 203
Duley, W. W., & Williams, D. A. 1981, MNRAS, 196, 269
Ehrenfreund, P., Robert, F., d'Hendecourt, L., & Behar, F. 1991, A&A, 252, 712
Field, D., Gerin, M., Leach, S., Lemaire, J. L., Pineau des Forêts, G., Rostas, F., Rouan, D., & Simons, D. 1994, A&A, 286, 909
Forst, W. 1973, Theory of Unimolecular Reactions (New York: Academic Press)
Gatley, I., et al. 1987, ApJ, 318, L73
Geballe, T. R., Joblin, C., d'Hendecourt, L. B., Jourdain de Muizon, M., Tielens, A. G. G. M., & Léger, A. 1994, ApJ, 434, L15
Geballe, T. R., Lacy, J. H., Persson, S. E., McGregor, P. J., & Soifer, B. T. 1985, ApJ, 292, 500
Geballe, T. R., Tielens, A. G. G. M., Allamandola, L. J., Moorhouse, A., & Brand, P. W. J. L. 1989, ApJ, 341, 278
Geballe, T. R., Tielens, A. G. G. M., Kwok, S., & Hrivnak, B. J. 1992, ApJ, 387, L89
Geballe, T. R., & van der Veen, W. E. C. J. 1990, A&A, 235, L9
Giard, M., Bernard, J. P., & Dennefeld, M. 1992, A&A, 264, 610
Guillois, O., Nenner, I., Papoular, R., & Reynaud, C. 1994, A&A, 285, 1003
Habing, H. J. 1968, Bull. Astron. Inst. Netherlands, 19, 421
Harvey, P. M., Wilking, B. A., & Joy, M. 1984, ApJ, 278, 156
Howe, J. E., Jaffe, D. T., Genzel, R., & Stacey, G. J. 1991, ApJ, 373, 158
Jaffe, D. T., Genzel, R., Harris, A. I., Howe, J. E., Stacey, G. J., & Stutzki, J. 1990, ApJ, 353, 193
Joblin, C. 1992, Ph.D. thesis, Université Paris 7
Joblin, C., Boissel, P., Léger, A., d'Hendecourt, L., & Défourneau, D. 1995a, A&A, 299, 835
Joblin, C., d'Hendecourt, L., & Léger, A. 1995b, in preparation
Jochims, H. W., Rühl, E., Baumgärtel, H., Tobita, S., & Leach, S. 1994, ApJ, 420, 307
Jourdain de Muizon, M., d'Hendecourt, L. B., & Geballe, T. R. 1990a, A&A, 227, 526
———. 1990b, A&A, 235, 367
Kiefer, J. H., Mizerka, L. J., Patel, M. R., & Wei, H. C. 1985, J. Phys. Chem., 89, 2013
Kurucz, R. L. 1979, ApJS, 40, 1
Léger, A., & Puget, J. L. 1984, A&A, 137, L5
Lowe, R. P., Moorhead, J. M., Wehlau, W. H., & Maillard, J. P. 1991, ApJ, 368, 195
Lutoshkin, V. I., Kotorlenko, L. A., & Krugylak, Y. A. 1972, Teor. Eksp. Khim., 8, 542
Papoular, R., Conard, J., Guiliano, M., Kister, J., & Mille, G. 1989, A&A, 217, 204
Papoular, R., Guillois, O., Nenner, I., & Reynaud, C. 1995, A&A, 293, 562
Pendleton, Y. J., Sandford, S. A., Allamandola, L. J., Tielens, A. G. G. M., & Sellgren, K. 1994, ApJ, 437, 683
Puget, J. L., & Léger, A. 1989, ARA&A, 27, 161
Puget, J. L., Léger, A., & d'Hendecourt, L. 1995, A&A, 293, 559
Sakata, A., Wada, S., Onaka, T., & Tokunaga, A. T. 1987, ApJ, 320, L63
Sakata, A., Wada, S., Tanabe, T., & Onaka, T. 1984, ApJ, 287, L51
Sandford, S. A. 1991, ApJ, 376, 599
Sandford, S. A., Allamandola, L. J., Tielens, A. G. G. M., Sellgren, K., Tapia, M., & Pendleton, Y. 1991, ApJ, 371, 607
Schutte, W. A., Tielens, A. G. G. M., & Allamandola, L. J. 1993, ApJ, 415, 397
Sellgren, K., Werner, M. W., & Dinerstein, H. L. 1983, ApJ, 271, L13
Steiman-Cameron, T., Haas, M. R., Tielens, A. G. G. M., & Burton, M. G. 1995, in preparation
Stein, S. E., Golden, D. M., & Benson, S. W. 1977, J. Phys. Chem., 81, 314
Tielens, A. G. G. M. 1993, in Dust and Chemistry in Astronomy, ed. T. J. Miller & D. H. Williams (Bristol: IOP), 99
Tielens, A. G. G. M., Allamandola, L. J., Barker, J. R., & Cohen, M. 1987, in Polycyclic Aromatic Hydrocarbons and Astrophysics, ed. A. Léger, L. d'Hendecourt, & N. Boccara (Dordrecht: Reidel), 99
Tielens, A. G. G. M., & Hollenbach, D. J. 1985, ApJ, 291, 722
Tielens, A. G. G. M., Meixner, M. M., van der Werf, P. P., Bregman, J., Tauber, J. A., Stutzki, J., & Rank, D. 1993, Science, 262, 86
Witt, A. N., & Malin, D. F. 1989, ApJ, 347, L25

Note added in proof.—The laboratory spectra presented here are for neutral PAHs, whereas the PAHs responsible for the interstellar emission features are thought to be ionized. The spectra of ionized PAHs resolve the relative intensity inconsistencies in the comparisons between the interstellar emission features and the earlier spectra at neutral PAHs (e.g., D. M. Hudgins & L. J. Allamandola, J. Phys. Chem., 99, 3033, [1995], and references therein). Although only a limited number of neutral PAHs with aliphatic side chains have been measured in the laboratory, the results are consistent with theoretical calculation of the spectra of a number of alkyl-substituted PAHs (S. R. Langhoff, unpublished).